



Article

Optical Constants and Structural Properties of Epitaxial MoS₂ Monolayers

Georgy A. Ermolaev ¹, Marwa A. El-Sayed ^{1,2}, Dmitry I. Yakubovskiy ¹, Kirill V. Voronin ^{1,3}, Roman I. Romanov ⁴, Mikhail K. Tatmyshevskiy ¹, Natalia V. Doroshina ¹, Anton B. Nemtsov ¹, Artem A. Voronov ¹, Sergey M. Novikov ¹, Andrey M. Markeev ¹, Gleb I. Tselikov ¹, Andrey A. Vyshnevyy ¹, Aleksey V. Arsenin ^{1,5} and Valentyn S. Volkov ^{1,5,*}

- ¹ Center for Photonics and 2D Materials, Moscow Institute of Physics and Technology, 9 Institutsky Lane, 141700 Dolgoprudny, Russia; georgiy.ermolaev@phystech.edu (G.A.E.); mira@phystech.edu (M.A.E.-S.); dmitrii.yakubovskii@phystech.edu (D.I.Y.); voronin.kv@phystech.edu (K.V.V.); mihailtatmyshev@inbox.ru (M.K.T.); doroshina.nv@phystech.edu (N.V.D.); nemtsov@phystech.edu (A.B.N.); voronov.aa@mipt.ru (A.A.V.); novikov.s@mipt.ru (S.M.N.); markeev.am@mipt.ru (A.M.M.); tselikov.gi@mipt.ru (G.I.T.); andrey.vyshnevyy@phystech.edu (A.A.V.); arsenin.av@mipt.ru (A.V.A.)
- ² Department of Physics, Faculty of Science, Menoufia University, Shebin El-Koom 32511, Egypt
- ³ Skolkovo Institute of Science and Technology, 3 Nobel Street, 143026 Moscow, Russia
- ⁴ Moscow Engineering Physics Institute, National Research Nuclear University MEPhI, 31 Kashirskoe Sh., 115409 Moscow, Russia; limpo2003@mail.ru
- ⁵ GrapheneTek, Skolkovo Innovation Center, 143026 Moscow, Russia
- * Correspondence: volkov.vs@mipt.ru; Tel.: +7-926-735-93-98



Citation: Ermolaev, G.A.; El-Sayed, M.A.; Yakubovskiy, D.I.; Voronin, K.V.; Romanov, R.I.; Tatmyshevskiy, M.K.; Doroshina, N.V.; Nemtsov, A.B.; Voronov, A.A.; Novikov, S.M.; et al. Optical Constants and Structural Properties of Epitaxial MoS₂ Monolayers. *Nanomaterials* **2021**, *11*, 1411. <https://doi.org/10.3390/nano11061411>

Academic Editors: Yann-Wen Lan and Der-Hsien Lien

Received: 3 May 2021
Accepted: 25 May 2021
Published: 27 May 2021

Publisher's Note: MDPI stays neutral with regard to jurisdictional claims in published maps and institutional affiliations.



Copyright: © 2021 by the authors. Licensee MDPI, Basel, Switzerland. This article is an open access article distributed under the terms and conditions of the Creative Commons Attribution (CC BY) license (<https://creativecommons.org/licenses/by/4.0/>).

Abstract: Two-dimensional layers of transition-metal dichalcogenides (TMDs) have been widely studied owing to their exciting potential for applications in advanced electronic and optoelectronic devices. Typically, monolayers of TMDs are produced either by mechanical exfoliation or chemical vapor deposition (CVD). While the former produces high-quality flakes with a size limited to a few micrometers, the latter gives large-area layers but with a nonuniform surface resulting from multiple defects and randomly oriented domains. The use of epitaxy growth can produce continuous, crystalline and uniform films with fewer defects. Here, we present a comprehensive study of the optical and structural properties of a single layer of MoS₂ synthesized by molecular beam epitaxy (MBE) on a sapphire substrate. For optical characterization, we performed spectroscopic ellipsometry over a broad spectral range (from 250 to 1700 nm) under variable incident angles. The structural quality was assessed by optical microscopy, atomic force microscopy, scanning electron microscopy, and Raman spectroscopy through which we were able to confirm that our sample contains a single-atomic layer of MoS₂ with a low number of defects. Raman and photoluminescence spectroscopies revealed that MBE-synthesized MoS₂ layers exhibit a two-times higher quantum yield of photoluminescence along with lower photobleaching compared to CVD-grown MoS₂, thus making it an attractive candidate for photonic applications.

Keywords: transition-metal dichalcogenides; MoS₂ monolayer; molecular beam epitaxy; optical constants; dielectric properties; refractive index; nanophotonics; spectroscopic ellipsometry

1. Introduction

The discovery of graphene as the first known 2D material [1] has generated a great momentum for research in nanoelectronics and nanophotonics based on low-dimensional materials [2–5]. Great efforts have been devoted to expanding the range of available materials. As a result, a new “periodic table” of 2D materials has been created, which comprises groups of transition metal chalcogenides (MX_n) [6,7], hexagonal boron nitride [8], monatomic materials, such as silicene, germanene, phosphorene, borophene [9–12], and a family of MXenes [13,14].

The family of transition metal dichalcogenides (TMDs) was widely recognized for the diversity of their electronic properties, encompassing superconductors [15], conductors [16,17], and semiconductors [18,19]. In addition to this vast diversity, materials can be stacked on each other, thus forming van der Waals heterostructures [19] and attaining novel properties. Furthermore, even monolayers of the same material can change their properties drastically when stacked to form twisted bilayers [20]. Thus, the use of TMDs allows one to design a large number of electronic, nanophotonic, mechanical, and thermal devices based only on 2D materials [6,21–24], making them inherently flexible and easy to use.

MoS₂ is a prominent representative of TMD semiconductors. When thinned down to a single atomic layer, it undergoes a transition from an indirect to a direct bandgap semiconductor [25], which is crucial for photonic applications as the radiative quantum yield drastically increases upon such transition [26]. In practice, monolayers of MoS₂ are typically obtained either via exfoliation or chemical vapor deposition (CVD). Both methods have serious drawbacks. Although exfoliated flakes have excellent structural and optical properties, their size is limited by a few microns, which hinders their commercial applications. CVD MoS₂ films overcome the size limitation, but at a price of decreased quality, both structural and optical. Recently, epitaxially grown films of TMDs [27], including MoS₂ [28], with a thickness down to a single atomic layer, have become available. Molecular beam epitaxy is a mature technology for the production of atomically smooth monocrystalline thin semiconductor films [29]; therefore, it has the potential to overcome size and quality limitations of exfoliation and CVD, respectively. At the same time, while the properties of CVD MoS₂ monolayers have been studied previously [30–34], little is known about the optical properties of available MBE-grown MoS₂ monolayers. Although recent works [27,35,36] report optical and electronic properties of MBE TMDs close to the exfoliated one, their epitaxial samples has at a maximum 200 μm lateral size, which is insufficient for the majority of applications [2–5]. To resolve this limitation, we focused on a large-scale MBE MoS₂, which covers more than 97% of the substrate surface.

Here we present a comprehensive study of the optical and structural properties of a MoS₂ monolayer grown by MBE on a sapphire substrate. Optical properties were measured by spectroscopic ellipsometry (SE) in a broad spectral range from 250 to 1700 nm. Using the Accurion EP4 imaging ellipsometer, which is capable of collecting the signal from a small micrometer-scaled area, we have measured optical constants of epitaxially grown monolayer MoS₂, and compared them with the available data of CVD-grown and exfoliated monolayer MoS₂ [37,38]. The structural properties of MoS₂ samples were assessed in a combined study comprising optical microscopy, scanning electron microscopy (SEM), atomic force microscopy (AFM), X-ray photoemission spectroscopy (XPS), Raman spectroscopy, and photoluminescence imaging. We find that MBE produces a polycrystalline monolayer film with a high crystallinity whose quantum yield of luminescence is higher than that of the CVD monolayers of MoS₂.

2. Results and Discussion

2.1. Sample Preparation and Characterization

Monolayers of MoS₂ were prepared through molecular beam epitaxy as schematically shown in Figure 1a. Before measurement, MoS₂ samples were washed and annealed in a vacuum chamber to remove any contaminants. The measured samples were uniform and high-crystalline as confirmed by images from optical, scanning electron microscopy (SEM), and atomic force microscopy (AFM) shown in Figure 1b–e. The epitaxial MoS₂ monolayer uniformly covers the double polished sapphire substrate with an average crystallite size of 6 μm, confirming the high quality of the samples [39]. Next, we validated that grown MoS₂ is atomically thin using AFM. The measured topography in Figure 1f yields 0.9 nm for film thickness, which is consistent with the previous results for monolayer MoS₂ [23,40–43].

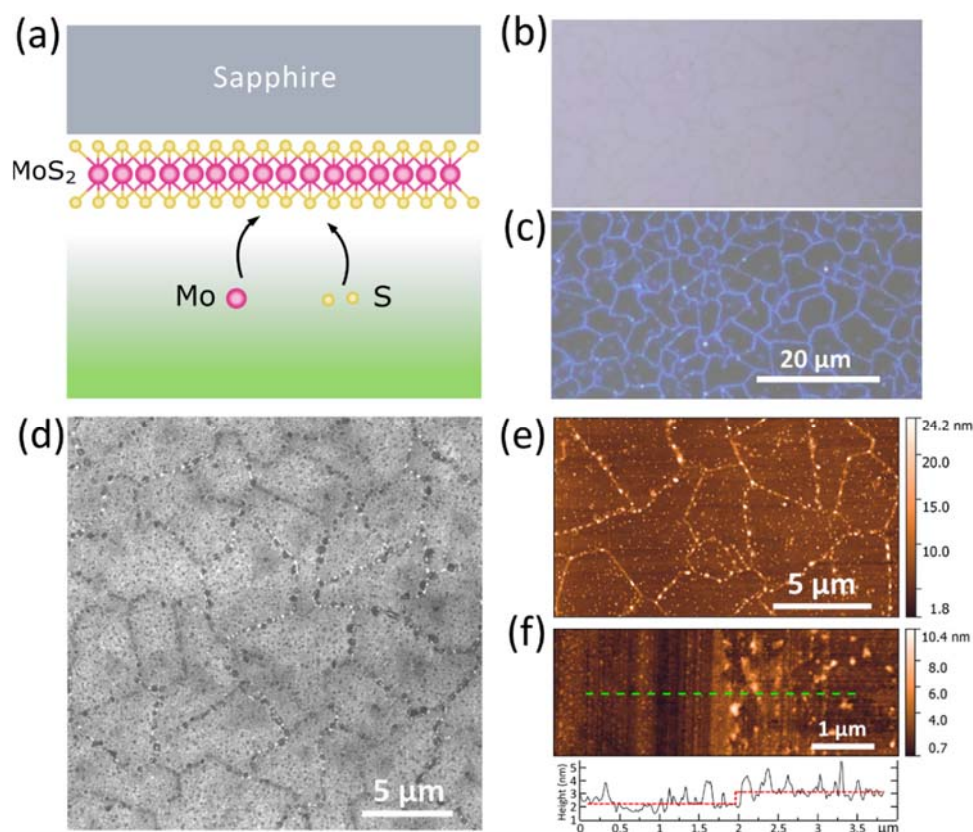


Figure 1. (a) A schematic diagram showing the concept of MBE growth monolayer MoS₂ on a sapphire substrate. (b,c) Optical image of the epitaxial MoS₂ taken in bright field (b) and dark field (c) regimes. MoS₂ covers more than 97% of the surface. (d) SEM image of the epitaxial MoS₂ revealing the high crystallinity of the samples with the characteristic crystallite size $6 \pm 2 \mu\text{m}$. (e) The AFM topography map of MoS₂ surface with a scan area of $17.5 \times 10 \mu\text{m}^2$. Root mean square roughness of MoS₂ is 0.5 nm in areas without defects. (f) The AFM topography map and the cross-sectional profile of the edge of epitaxial MoS₂ along the green line, giving the MoS₂ layer thickness of $\sim 0.9 \text{ nm}$. The scan area was $5.5 \times 2 \mu\text{m}^2$.

We carried out a detailed comparison of photoluminescence and Raman spectra for epitaxial and CVD-grown MoS₂ monolayers for further investigation of the samples' quality. Photoluminescence (PL) of the CVD and epitaxial monolayer MoS₂ grown on sapphire substrates are presented in Figure 2a. PL was excited resonantly at 632.8 nm. Each spectrum was deconvoluted into two Gaussian peaks with maxima at about 1.87 and 1.8 eV in the case of CVD-grown MoS₂ and 1.85 and 1.78 eV in MBE-synthesized MoS₂. The first peak A corresponds to the radiative excitonic recombination while the microscopic origin of the second peak remains a disputable topic. Earlier works attribute it to negatively charged trions [44,45] related to n-type conductivity, while a more recent work [46] argues that it stems from the recombination of bound excitons formed on either the unintended impurities or the native point defects. Regardless of the PL mechanism (bound excitons or trions) of the peak, in both cases it comes from structural defects of the sample, since inherent n-type conductivity can originate only from defects [47] or donor impurities. Hence, the defect's contribution into PL spectrum is 14% for epitaxial MoS₂ and 22% for CVD MoS₂, thereby validating the lower density of structural defects in MBE MoS₂. Moreover, A-exciton PL is almost two times brighter for MBE MoS₂ compared to the CVD sample, as is clearly seen in Figure 2a. Additionally, PL from epitaxial MoS₂ has a 0.025 eV red-shift in respect to the CVD sample, which implies that MBE MoS₂ has a slightly different crystal structure. The non-resonant Raman scattering spectra of the CVD and the epitaxial monolayer MoS₂ grown on sapphire substrates are presented in Figure 2b.

The Mo3d spectrum was decomposed of two doublets, with the more intense one corresponding to the Mo⁴⁺ state in the MoS₂ compound. The less intense doublet corresponded to the Mo⁶⁺ state in the MoO₃ compound. In addition, the S2s and “loss feature” lines were present in the spectra. The position of the Mo3d5/2 line for the CVD MoS₂ and MBE MoS₂ samples was 229.8 eV and 229.4 eV, respectively. The difference in the position of the lines could be caused by different levels of doping. The molybdenum fraction in the Mo6+ state for CVD MoS₂ and MBE MoS₂ samples was 0.10 and 0.18, respectively. The total atomic concentration ratio [S]/[Mo] for CVD MoS₂ and MBE MoS₂ samples was 1.8 and 1.7, respectively. No noticeable concentration of other impurities was observed in XPS measurements. The natural oxidation of single-layered MoS₂ under ambient conditions has been previously reported [49] and the S vacancies are formed through oxidation spontaneously followed by an O substitution process since the oxidation is thermodynamically more favorable [50,51]. The results of XPS measurements indicate that the increased photoluminescence yield of MBE MoS₂ might be due to the passivation of sulfur vacancies and crystallite boundaries by oxygen [52].

2.2. Dielectric Response Analysis

The dielectric response of MBE MoS₂ was determined using spectroscopic ellipsometry (SE), and the resulting spectra are shown in Figure 4a,b. The ellipsometric parameter Ψ clearly reveals MoS₂ excitonic features, which we described through the Tauc-Lorentz oscillator model [38] with their resulting parameters collected in Table 1. Figure 4c depicts the corresponding dielectric function. Notably, the optical bandgap of the MBE sample equals 1.718 eV, while for CVD MoS₂ this value is 1.744 eV [39]. This red-shift (0.026 eV) of optical bandgap is in agreement with the PL result (0.025 eV) from Figure 2a. We also recorded transmission spectra and compared them to the transfer matrix calculations [53] to verify the extracted dielectric response in Figure 4c and confirm its predictive capability. The measured and calculated transmittance spectra plotted in Figure 4d match perfectly, thus validating our result in Figure 4c.

Interestingly, the optical constants of MBE MoS₂ are intermediate between CVD and exfoliated MoS₂, as illustrated in Figure 4c. For example, at λ = 750 nm the refractive index of CVD, MBE, and exfoliated MoS₂ are 3.2, 4.0, and 5.2, respectively. Therefore, the MBE growth technique allows getting closer to superior properties of exfoliated MoS₂, but at a large scale. It makes MBE MoS₂ a promising platform for scientific and industrial photonic applications.

Table 1. Tauc-Lorentz parameters of the oscillators (excitons) with ε_∞ = 0.54 used to describe dielectric function of MBE MoS₂.

Oscillator	A (eV)	C (meV)	E _g (eV)	E ₀ (eV)
#1	410	120	1.718	1.787
#2	84	88	1.832	1.955
#3	77	600	1.565	2.872
#4	80	731	2.856	4.070
#5	281	826	4.135	4.504

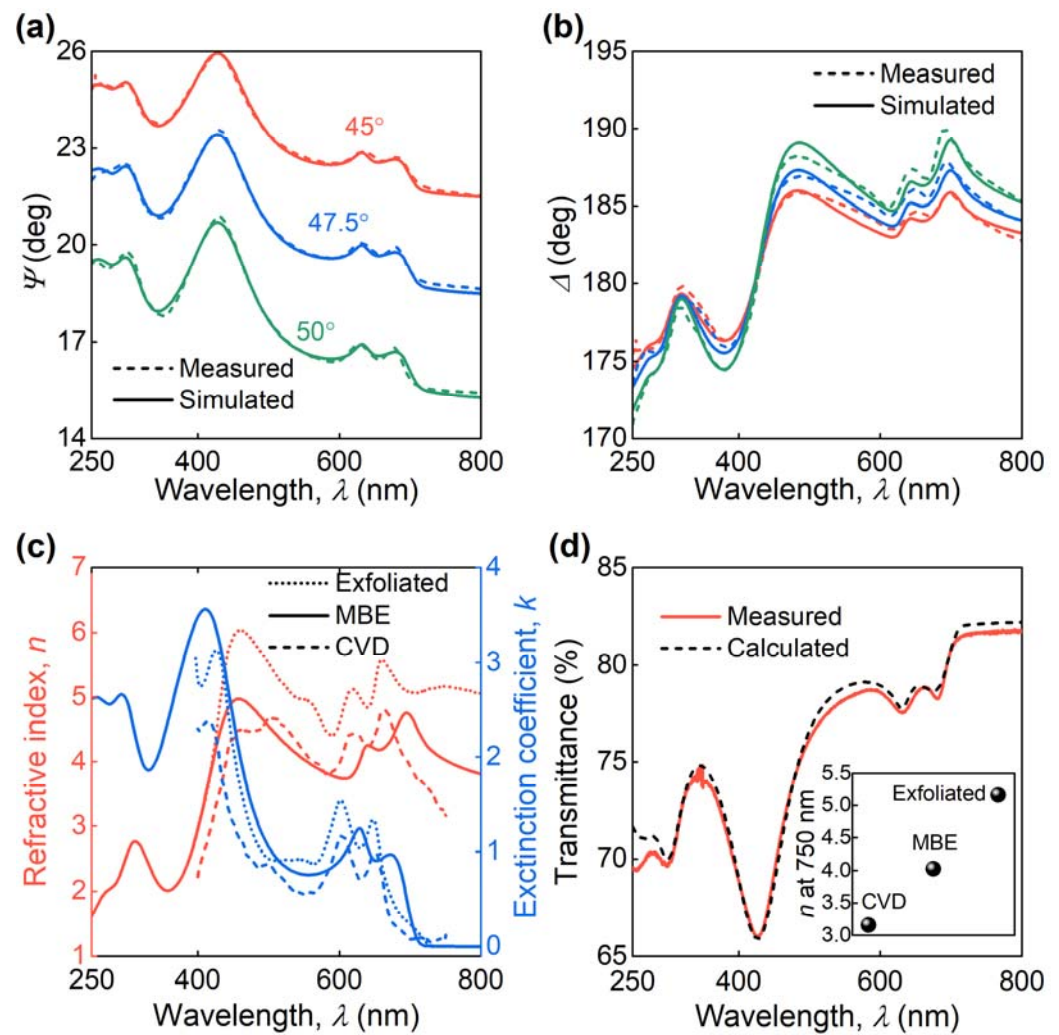


Figure 4. Optical properties of MBE MoS₂. Plots of the measured and calculated MBE MoS₂ ellipsometric parameters (a) Ψ and (b) Δ . (c) Optical constants (n and k) of epitaxial monolayer MoS₂ grown on a sapphire substrate from SE analysis of panels (a,b). For the tabular data, see Table A1. For comparison, we added optical constants of CVD and exfoliated MoS₂ from ref. [37,38], respectively. (d) Measured (red line) and calculated (black line) transmittance spectra of MBE MoS₂ on sapphire matching perfectly within spectrophotometer accuracy (1%) except in the 250–270 nm range, where inaccuracy approaches 2% attributed to the low signal sensitivity of our ellipsometer in that interval. The inset is a refractive index of exfoliated, MBE, and CVD MoS₂ at 750 nm.

The difference in the optical properties of MBE-synthesized MoS₂ films from films fabricated by other methods must be taken into account when developing optical devices, since the difference in optical constants entails differences in characteristics of the device. To illustrate this, we consider a biosensor based on surface plasmon resonance in the Kretschmann scheme [54], in which a thin gold film covers a silicon oxide prism, and the change in the refraction index is detected by measuring the change of the resonant angle, at which the reflection from the scheme is minimal. To increase the sensitivity and coupling with the studied molecules, several layers of van der Waals material, such as graphene, are often deposited on the gold surface [55,56]. The addition of layers of molybdenum disulfide also improves the sensitivity of the biosensor. Figure 5 shows the dependence of the reflection coefficient on the angle of incidence (Figure 5a) and the dependence of the biosensor sensitivity on the number of MoS₂ layers (Figure 5b). The calculations were performed for a wavelength of 635 nm, which is often used in optical biosensors, with a gold thickness of 40 nm. It turns out that even for a couple of MoS₂ layers, both the

dependence of the reflection coefficient on the angle of incidence and the sensitivity of the biosensor differ by more than 10% for MoS₂ films obtained by different methods. As a result, fabrication technology provides an efficient way to control the dielectric function of MoS₂, and hence, a method to tailor the optical response in photonic applications.

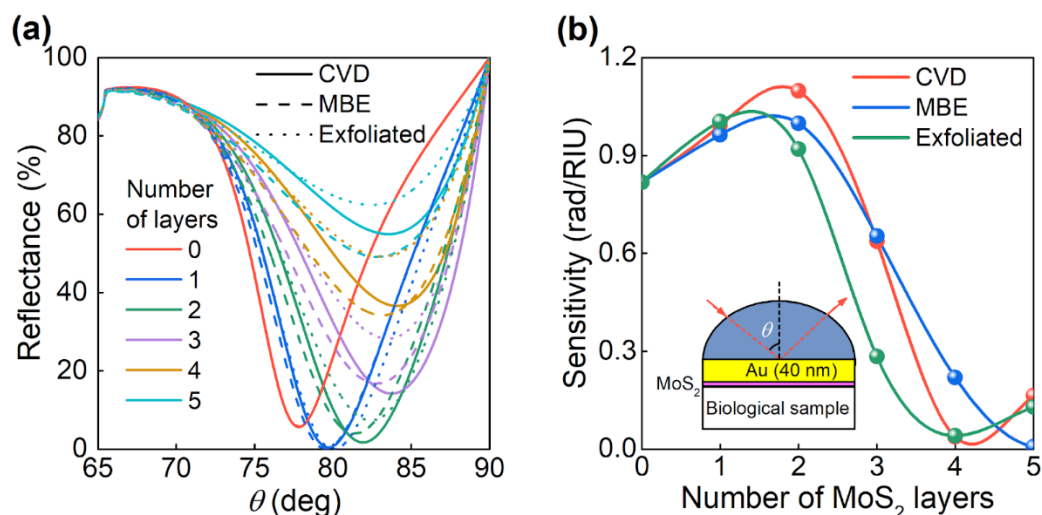


Figure 5. Surface plasmonic resonance (SPR) sensor based on SiO₂/Au (40 nm) chip with CVD, MBE and exfoliated MoS₂. (a) The reflectance of SPR sensor for different layer numbers of CVD, MBE, and exfoliated MoS₂. (b) The dependence of the SPR sensor sensitivity on the MoS₂ number of layers. The inset is a scheme of an SPR sensor.

3. Materials and Methods

3.1. Materials

Isolated triangles with some full coverage areas of epitaxial MoS₂ monolayer samples were purchased from 2d Semiconductors, Inc. (<https://www.2dsemiconductors.com/>) (accessed on 25 May 2021), Scottsdale, AZ, USA). Samples were grown in an MBE chamber at a base pressure of 8×10^{-9} Torr on a double-side polished c-cut sapphire. An extremely slow deposition rate of 5–100 atoms per second provides a single-crystal quality film deposition with a high crystallinity and reduced defect density. CVD-grown full area coverage monolayer MoS₂ samples purchased from the SixCarbon Technology (<http://www.6carbon.com/>) (accessed on 25 May 2021), Shenzhen, China) were synthesized with atmospheric pressure chemical vapor deposition also on double-side polished c-cut sapphire.

3.2. Raman and Photoluminescence Characterization

The experimental setup used for Raman measurements was a confocal scanning Raman microscope Horiba LabRAM HR Evolution (HORIBA Ltd., Kyoto, Japan). All measurements were carried out using linearly polarized excitation at wavelengths 532 and 632.8 nm, 1800 lines/mm diffraction grating, and $\times 100$ objective with a numerical aperture of 0.9. Meanwhile, we used unpolarized detection to have a significant signal-to-noise ratio. The spot size was $\sim 0.43 \mu\text{m}$. The Raman spectra were recorded with 0.75 mW (wavelength 632.8 nm) and 1.5 mW (wavelength 532 nm) incident power and an integration time of 3 s at each point. To compare CVD and epitaxial MoS₂ PL response, we normalized PL spectra to A_{1g}(Γ) Raman peak since they recorded simultaneously. The statistics were collected with at least 15 points for each sample, and the observed variation of the intensity for the spectra was less than 5%.

3.3. X-ray Photoemission Spectroscopy Characterization

For the detailed study of the CVD and epitaxial MoS₂ monolayers grown on sapphire substrates, we performed measurements of the Mo3d and S2p5/2 level X-ray photoemission spectroscopy (XPS) spectra to reveal the difference in the elemental composition of two samples (Thermo Scientific K-Alpha, Waltham, MA, USA). Since the MoS₂ samples on sapphire substrates were charged during the XPS measurements, the charge-compensation mode was used. The calibration was performed using the C1s line position at 284.5 eV.

3.4. Atomic Force Microscopy, Optical Visualization, Scanning Electron Microscopy

The roughness and homogeneity of the epitaxial MoS₂ monolayer were measured by an atomic force microscope (NT-MDT Ntegra, Moscow, Russia). The MoS₂ MBE fabricated sample was characterized immediately after unsealing without any pollution at ambient conditions, and thus these defects demonstrated in AFM and SEM in Figure 1d–f are the result of an MBE fabrication procedure. These defects might be Mo nucleation sites. The surface images (2400 × 2400 pixels) of the MoS₂ samples were captured by an optical microscope (Nikon LV150, Tokyo, Japan) with a digital camera DS-Fi3. To investigate the MoS₂ surface morphology, we additionally used the scanning electron microscope using the acceleration voltage of 3 kV (JEOL JSM-7001F, Tokyo, Japan).

3.5. Ellipsometry Characterization

Spectroscopic ellipsometry was conducted at several incident angles (45°, 47.5°, 50°) over a wide spectral range of 250 to 1700 nm (0.73–4.96 eV). An imaging ellipsometer in the rotation compensator mode was used for the measurements (Accurion nanofilm_ep4, Goettingen, Germany). We used the Tauc-Lorentz oscillator model for ellipsometry spectra analysis following the analysis algorithm developed by Ermolaev and colleagues [39,40]. The Tauc-Lorentz oscillator model is defined as:

$$\varepsilon_2 = \begin{cases} \frac{1}{E} \cdot \frac{AE_0C(E-E_g)^2}{(E^2-E_0^2)^2+C^2E^2} & \text{for } E > E_g \\ 0 & \text{for } E < E_g \end{cases},$$

where E is the photon energy, A is the strength of the oscillator, C is the broadening term, E_g is the optical band gap, and E_0 is the peak central energy. The real part ε_1 of the dielectric function is derived from the expression of imaginary part ε_2 of the dielectric function using the Kramers–Kronig integration.

4. Conclusions

To summarize, we have performed a detailed study of the structural and optical properties of monolayer MoS₂ synthesized by MBE. We verified that the sample indeed contains a single-atomic layer of MoS₂ through Raman and AFM measurements, while XPS measurements confirmed its high purity. The high crystallinity of the sample with a characteristic crystallite size of 6 μm was revealed by SEM, AFM imaging and dark-field microscopy. The quantum yield of MBE MoS₂ by almost two times exceeds that of CVD MoS₂, as demonstrated by PL measurements, which proves its superior qualities for active photonic applications. Finally, we have conducted accurate measurements of optical constants of MBE MoS₂ by spectroscopic ellipsometry. The accuracy of the optical properties has been further verified by the measurement of the optical transmittance spectrum, which fully agrees with calculations based on the optical constants acquired by ellipsometry. Additionally, we demonstrated the significance of our accurate measurements for practical applications by comparing characteristics of SPR sensors calculated using the different constants. Even devices with only a few atomic layers of MoS₂ demonstrate substantial differences in sensitivity and anticipated signal intensity when different sources of optical properties are used. Our results create a firm ground for photonic applications of atomically thin layers of transition metal dichalcogenides.

Author Contributions: G.A.E., M.A.E.-S., K.V.V., S.M.N., A.M.M., G.I.T., A.A.V. (Andrey A. Vyshnevyy), A.V.A. and V.S.V. proposed the concept, conceived and designed the experiments and wrote original draft. G.A.E., M.A.E.-S., D.I.Y., R.I.R., M.K.T., N.V.D., A.B.N., A.A.V. (Artem A. Voronov), S.M.N. and G.I.T. performed the measurements and analyzed the data. K.V.V. and A.A.V. (Andrey A. Vyshnevyy) provided theoretical support. All authors discussed the results and contributed to manuscript preparation. G.A.E. and M.A.E.-S. contributed equally to this work and should be considered co-first authors. All authors have read and agreed to the published version of the manuscript.

Funding: The experimental work was supported by the Russian Science Foundation, grant No. 19-79-00350. The numerical analysis of multilayer structures was supported by the Russian Science Foundation, grant No. 20-79-00349.

Institutional Review Board Statement: Not applicable.

Informed Consent Statement: Not applicable.

Data Availability Statement: The data presented in this study are available on request from the corresponding author.

Acknowledgments: The authors thank the MIPT's Shared Research Facilities Center for the use of their equipment.

Conflicts of Interest: The authors declare no conflict of interest.

Appendix A

Table A1. Tabulated optical constants for epitaxial MoS₂ monolayer on sapphire substrates.

λ (nm)	n	k
250	1.60684	2.61054
275	2.02921	2.55685
300	2.56575	2.58710
325	2.55812	1.89351
350	2.04339	2.16150
375	2.17595	2.89179
400	2.95143	3.48336
425	4.18875	3.38186
450	4.93334	2.40006
475	4.85958	1.51647
500	4.55210	1.04876
525	4.26415	0.83499
550	4.03556	0.75964
575	3.86255	0.77777
600	3.74944	0.90252
625	3.90919	1.22200
650	4.20291	0.90721
675	4.38497	0.96487
700	4.71574	0.32016
725	4.23306	0.00662
750	4.02327	0.00250
775	3.89866	0.00000
800	3.80981	0.00000
825	3.74192	0.00000
850	3.68740	0.00000
875	3.64225	0.00000
900	3.60403	0.00000
925	3.57116	0.00000
950	3.54254	0.00000
975	3.52215	0.00000

Table A1. Cont.

λ (nm)	n	k
1000	3.49502	0.00000
1025	3.47888	0.00000
1050	3.45713	0.00000
1075	3.44403	0.00000
1100	3.42620	0.00000
1125	3.41536	0.00000
1150	3.40050	0.00000
1175	3.39140	0.00000
1200	3.37883	0.00000
1225	3.37110	0.00000
1250	3.36035	0.00000
1275	3.35371	0.00000
1300	3.34443	0.00000
1325	3.33867	0.00000
1350	3.33059	0.00000
1375	3.32556	0.00000
1400	3.31847	0.00000
1425	3.31404	0.00000
1450	3.30779	0.00000
1475	3.30387	0.00000
1500	3.29832	0.00000
1525	3.29482	0.00000
1550	3.28987	0.00000
1575	3.28674	0.00000
1600	3.28674	0.00000
1625	3.27949	0.00000
1650	3.27549	0.00000
1675	3.27296	0.00000
1700	3.26934	0.00000

References

- Novoselov, K.S.; Geim, A.K.; Morozov, S.V.; Jiang, D.; Zhang, Y.; Dubonos, S.V.; Grigorieva, I.V.; Firsov, A.A. Electric Field Effect in Atomically Thin Carbon Films. *Science* **2004**, *306*, 666–669. [[CrossRef](#)] [[PubMed](#)]
- Novoselov, K.S.; Mishchenko, A.; Carvalho, A.; Castro Neto, A.H. 2D Materials and van Der Waals Heterostructures. *Science* **2016**, *353*, aac9439. [[CrossRef](#)]
- Mak, K.F.; Shan, J. Photonics and Optoelectronics of 2D Semiconductor Transition Metal Dichalcogenides. *Nat. Photonics* **2016**, *10*, 216–226. [[CrossRef](#)]
- Datta, I.; Chae, S.H.; Bhatt, G.R.; Tadayon, M.A.; Li, B.; Yu, Y.; Park, C.; Park, J.; Cao, L.; Basov, D.N.; et al. Low-Loss Composite Photonic Platform Based on 2D Semiconductor Monolayers. *Nat. Photonics* **2020**, *14*, 256–262. [[CrossRef](#)]
- Tan, C.; Cao, X.; Wu, X.-J.; He, Q.; Yang, J.; Zhang, X.; Chen, J.; Zhao, W.; Han, S.; Nam, G.-H.; et al. Recent Advances in Ultrathin Two-Dimensional Nanomaterials. *Chem. Rev.* **2017**, *117*, 6225–6331. [[CrossRef](#)] [[PubMed](#)]
- Wang, Q.H.; Kalantar-Zadeh, K.; Kis, A.; Coleman, J.N.; Strano, M.S. Electronics and Optoelectronics of Two-Dimensional Transition Metal Dichalcogenides. *Nat. Nanotechnol.* **2012**, *7*, 699–712. [[CrossRef](#)]
- Peng, B.; Ang, P.K.; Loh, K.P. Two-Dimensional Dichalcogenides for Light-Harvesting Applications. *Nano Today* **2015**, *10*, 128–137. [[CrossRef](#)]
- Caldwell, J.D.; Aharonovich, I.; Cassabois, G.; Edgar, J.H.; Gil, B.; Basov, D.N. Photonics with Hexagonal Boron Nitride. *Nat. Rev. Mater.* **2019**, *4*, 552–567. [[CrossRef](#)]
- Li, D.; Gao, J.; Cheng, P.; He, J.; Yin, Y.; Hu, Y.; Chen, L.; Cheng, Y.; Zhao, J. 2D Boron Sheets: Structure, Growth, and Electronic and Thermal Transport Properties. *Adv. Funct. Mater.* **2020**, *30*, 1904349. [[CrossRef](#)]
- Ambrosi, A.; Sofer, Z.; Pumera, M. Electrochemical Exfoliation of Layered Black Phosphorus into Phosphorene. *Angew. Chem. Int. Ed Engl.* **2017**, *56*, 10443–10445. [[CrossRef](#)]
- Fleurence, A.; Friedlein, R.; Ozaki, T.; Kawai, H.; Wang, Y.; Yamada-Takamura, Y. Experimental Evidence for Epitaxial Silicene on Diboride Thin Films. *Phys. Rev. Lett.* **2012**, *108*, 245501. [[CrossRef](#)] [[PubMed](#)]
- Dávila, M.E.; Xian, L.; Cahangirov, S.; Rubio, A.; Le Lay, G. Germanene: A Novel Two-Dimensional Germanium Allotrope Akin to Graphene and Silicene. *New J. Phys.* **2014**, *16*, 095002. [[CrossRef](#)]
- Naguib, M.; Mochalin, V.N.; Barsoum, M.W.; Gogotsi, Y. 25th Anniversary Article: MXenes: A New Family of Two-Dimensional Materials. *Adv. Mater.* **2014**, *26*, 992–1005. [[CrossRef](#)]

14. Jiang, X.; Kuklin, A.V.; Baev, A.; Ge, Y.; Ågren, H.; Zhang, H.; Prasad, P.N. Two-Dimensional MXenes: From Morphological to Optical, Electric, and Magnetic Properties and Applications. *Phys. Rep.* **2020**, *848*, 1–58. [[CrossRef](#)]
15. Saito, Y.; Nojima, T.; Iwasa, Y. Highly Crystalline 2D Superconductors. *Nat. Rev. Mater.* **2017**, *2*, 16094. [[CrossRef](#)]
16. da Jornada, F.H.; Xian, L.; Rubio, A.; Louie, S.G. Universal Slow Plasmons and Giant Field Enhancement in Atomically Thin Quasi-Two-Dimensional Metals. *Nat. Commun.* **2020**, *11*, 1013. [[CrossRef](#)]
17. Zhao, S.; Hotta, T.; Koretsune, T.; Watanabe, K.; Taniguchi, T.; Sugawara, K.; Takahashi, T.; Shinohara, H.; Kitaura, R. Two-Dimensional Metallic NbS₂: Growth, Optical Identification and Transport Properties. *2D Mater.* **2016**, *3*, 025027. [[CrossRef](#)]
18. Radisavljevic, B.; Radenovic, A.; Brivio, J.; Giacometti, V.; Kis, A. Single-Layer MoS₂ Transistors. *Nat. Nanotechnol.* **2011**, *6*, 147–150. [[CrossRef](#)]
19. Geim, A.K.; Grigorieva, I.V. Van Der Waals Heterostructures. *Nature* **2013**, *499*, 419–425. [[CrossRef](#)]
20. Scuri, G.; Andersen, T.I.; Zhou, Y.; Wild, D.S.; Sung, J.; Gelly, R.J.; Bérubé, D.; Heo, H.; Shao, L.; Joe, A.Y.; et al. Electrically Tunable Valley Dynamics in Twisted WSe₂/WSe₂ Bilayers. *Phys. Rev. Lett.* **2020**, *124*, 217403. [[CrossRef](#)]
21. Jariwala, D.; Sangwan, V.K.; Lauhon, L.J.; Marks, T.J.; Hersam, M.C. Emerging Device Applications for Semiconducting Two-Dimensional Transition Metal Dichalcogenides. *ACS Nano* **2014**, *8*, 1102–1120. [[CrossRef](#)]
22. Choi, W.; Choudhary, N.; Han, G.H.; Park, J.; Akinwande, D.; Lee, Y.H. Recent Development of Two-Dimensional Transition Metal Dichalcogenides and Their Applications. *Mater. Today* **2017**, *20*, 116–130. [[CrossRef](#)]
23. Yakubovsky, D.I.; Stebunov, Y.V.; Kirtaev, R.V.; Ermolaev, G.A.; Mironov, M.S.; Novikov, S.M.; Arsenin, A.V.; Volkov, V.S. Ultrathin and Ultrasoother Gold Films on Monolayer MoS₂. *Adv. Mater. Interfaces* **2019**, *6*, 1900196. [[CrossRef](#)]
24. Ermolaev, G.A.; Grudin, D.V.; Stebunov, Y.V.; Voronin, K.V.; Kravets, V.G.; Duan, J.; Mazitov, A.B.; Tselikov, G.I.; Bylinkin, A.; Yakubovsky, D.I.; et al. Giant Optical Anisotropy in Transition Metal Dichalcogenides for next-Generation Photonics. *Nat. Commun.* **2021**, *12*, 854. [[CrossRef](#)] [[PubMed](#)]
25. Mak, K.F.; Lee, C.; Hone, J.; Shan, J.; Heinz, T.F. Atomically Thin MoS₂: A New Direct-Gap Semiconductor. *Phys. Rev. Lett.* **2010**, *105*, 136805. [[CrossRef](#)]
26. Amani, M.; Lien, D.-H.; Kiriya, D.; Xiao, J.; Azcatl, A.; Noh, J.; Madhupathy, S.R.; Addou, R.; Kc, S.; Dubey, M.; et al. Near-Unity Photoluminescence Quantum Yield in MoS₂. *Science* **2015**, *350*, 1065–1068. [[CrossRef](#)]
27. Choudhury, T.H.; Zhang, X.; Al Balushi, Z.Y.; Chubarov, M.; Redwing, J.M. Epitaxial Growth of Two-Dimensional Layered Transition Metal Dichalcogenides. *Annu. Rev. Mater. Res.* **2020**, *50*, 155–177. [[CrossRef](#)]
28. El Kazzi, S.; Mortelmans, W.; Nuytten, T.; Meerssaut, J.; Carolan, P.; Landeloos, L.; Conard, T.; Radu, I.; Heyns, M.; Merckling, C. MoS₂ Synthesis by Gas Source MBE for Transition Metal Dichalcogenides Integration on Large Scale Substrates. *J. Appl. Phys.* **2018**, *123*, 135702. [[CrossRef](#)]
29. Chang, L.L.; Ploog, K. (Eds.) *Molecular Beam Epitaxy and Heterostructures*; NATO ASI Series; Springer: Dordrecht, The Netherlands, 1985; ISBN 9789024731183.
30. Li, W.; Birdwell, A.G.; Amani, M.; Burke, R.A.; Ling, X.; Lee, Y.-H.; Liang, X.; Peng, L.; Richter, C.A.; Kong, J.; et al. Broadband Optical Properties of Large-Area Monolayer CVD Molybdenum Disulfide. *Phys. Rev. B* **2014**, *90*, 195434. [[CrossRef](#)]
31. Liu, H.-L.; Shen, C.-C.; Su, S.-H.; Hsu, C.-L.; Li, M.-Y.; Li, L.-J. Optical Properties of Monolayer Transition Metal Dichalcogenides Probed by Spectroscopic Ellipsometry. *Appl. Phys. Lett.* **2014**, *105*, 201905. [[CrossRef](#)]
32. Kravets, V.G.; Prorok, V.V.; Poperenko, L.V.; Shaykevich, I.A. Ellipsometry and Optical Spectroscopy of Low-Dimensional Family TMDs. *Semicond. Phys. Quantum Electron. Optoelectron.* **2017**, *20*, 284–296. [[CrossRef](#)]
33. Ghasemi, F.; Frisenda, R.; Dumcenco, D.; Kis, A.; Perez de Lara, D.; Castellanos-Gomez, A. High Throughput Characterization of Epitaxially Grown Single-Layer MoS₂. *Electronics* **2017**, *6*, 28. [[CrossRef](#)]
34. Yu, Y.; Yu, Y.; Cai, Y.; Li, W.; Gurarslan, A.; Peelaers, H.; Aspnes, D.E.; Van de Walle, C.G.; Nguyen, N.V.; Zhang, Y.-W.; et al. Exciton-Dominated Dielectric Function of Atomically Thin MoS₂ Films. *Sci. Rep.* **2015**, *5*, 16996. [[CrossRef](#)] [[PubMed](#)]
35. Fu, D.; Zhao, X.; Zhang, Y.-Y.; Li, L.; Xu, H.; Jang, A.-R.; Yoon, S.I.; Song, P.; Poh, S.M.; Tianhua, R.; et al. Molecular Beam Epitaxy of Highly Crystalline Monolayer Molybdenum Disulfide on Hexagonal Boron Nitride. *J. Am. Chem. Soc.* **2017**, *139*, 9392–9400. [[CrossRef](#)]
36. Pacuski, W.; Grzeszczyk, M.; Nogajewski, K.; Bogucki, A.; Oreszczuk, K.; Kucharek, J.; Polczynska, K.E.; Sredynski, B.; Rodek, A.; Bozek, R.; et al. Narrow Excitonic Lines and Large-Scale Homogeneity of Transition-Metal Dichalcogenide Monolayers Grown by Molecular Beam Epitaxy on Hexagonal Boron Nitride. *Nano Lett.* **2020**, *20*, 3058–3066. [[CrossRef](#)] [[PubMed](#)]
37. Zhang, H.; Ma, Y.; Wan, Y.; Rong, X.; Xie, Z.; Wang, W.; Dai, L. Measuring the Refractive Index of Highly Crystalline Monolayer MoS₂ with High Confidence. *Sci. Rep.* **2015**, *5*, 8440. [[CrossRef](#)]
38. Hsu, C.; Frisenda, R.; Schmidt, R.; Arora, A.; Vasconcellos, S.M.; Bratschitsch, R.; Zant, H.S.J.; Castellanos-Gomez, A. Thickness-Dependent Refractive Index of 1L, 2L, and 3L MoS₂, MoSe₂, WS₂, and WSe₂. *Adv. Opt. Mater.* **2019**, *7*, 1900239. [[CrossRef](#)]
39. Ermolaev, G.A.; Stebunov, Y.V.; Vyshnevyy, A.A.; Tatarkin, D.E.; Yakubovsky, D.I.; Novikov, S.M.; Baranov, D.G.; Shegai, T.; Nikitin, A.Y.; Arsenin, A.V.; et al. Broadband Optical Properties of Monolayer and Bulk MoS₂. *npj 2D Mater. Appl.* **2020**, *4*, 21. [[CrossRef](#)]
40. Ermolaev, G.A.; Yakubovsky, D.I.; Stebunov, Y.V.; Arsenin, A.V.; Volkov, V.S. Spectral Ellipsometry of Monolayer Transition Metal Dichalcogenides: Analysis of Excitonic Peaks in Dispersion. *J. Vac. Sci. Technol. B Nanotechnol. Microelectron.* **2020**, *38*, 014002. [[CrossRef](#)]

41. Tao, L.; Long, H.; Zhou, B.; Yu, S.F.; Lau, S.P.; Chai, Y.; Fung, K.H.; Tsang, Y.H.; Yao, J.; Xu, D. Preparation and Characterization of Few-Layer MoS₂ Nanosheets and Their Good Nonlinear Optical Responses in the PMMA Matrix. *Nanoscale* **2014**, *6*, 9713–9719. [[CrossRef](#)]
42. Lee, C.; Yan, H.; Brus, L.E.; Heinz, T.F.; Hone, J.; Ryu, S. Anomalous Lattice Vibrations of Single- and Few-Layer MoS₂. *ACS Nano* **2010**, *4*, 2695–2700. [[CrossRef](#)]
43. Li, H.; Wu, J.; Huang, X.; Lu, G.; Yang, J.; Lu, X.; Xiong, Q.; Zhang, H. Rapid and Reliable Thickness Identification of Two-Dimensional Nanosheets Using Optical Microscopy. *ACS Nano* **2013**, *7*, 10344–10353. [[CrossRef](#)] [[PubMed](#)]
44. Lu, Y.; Chen, T.; Ryu, G.H.; Huang, H.; Sheng, Y.; Chang, R.-J.; Warner, J.H. Self-Limiting Growth of High-Quality 2D Monolayer MoS₂ by Direct Sulfurization Using Precursor-Soluble Substrates for Advanced Field-Effect Transistors and Photodetectors. *ACS Appl. Nano Mater.* **2019**, *2*, 369–378. [[CrossRef](#)]
45. Mak, K.F.; He, K.; Lee, C.; Lee, G.H.; Hone, J.; Heinz, T.F.; Shan, J. Tightly bound trions in monolayer MoS₂. *Nat. Mater.* **2013**, *12*, 207–211. [[CrossRef](#)] [[PubMed](#)]
46. Kaplan, D.; Gong, Y.; Mills, K.; Swaminathan, V.; Ajayan, P.M.; Shirodkar, S.; Kaxiras, E. Excitation Intensity Dependence of Photoluminescence from Monolayers of MoS₂ and WS₂ /MoS₂ Heterostructures. *2D Mater.* **2016**, *3*, 015005. [[CrossRef](#)]
47. McDonnell, S.; Addou, R.; Buie, C.; Wallace, R.M.; Hinkle, C.L. Defect-Dominated Doping and Contact Resistance in MoS₂. *ACS Nano* **2014**, *8*, 2880–2888. [[CrossRef](#)] [[PubMed](#)]
48. Chakraborty, B.; Ramakrishna Matte, H.S.; Sood, A.K.; Rao, C.N.R. Layer-Dependent Resonant Raman Scattering of a Few Layer MoS₂. *J. Raman Spectrosc.* **2013**, *44*, 92–96. [[CrossRef](#)]
49. Gao, J.; Li, B.; Tan, J.; Chow, P.; Lu, T.-M.; Koratkar, N. Aging of Transition Metal Dichalcogenide Monolayers. *ACS Nano* **2016**, *10*, 2628–2635. [[CrossRef](#)] [[PubMed](#)]
50. Longo, R.C.; Addou, R.; Santosh, K.C.; Noh, J.-Y.; Smyth, C.M.; Barrera, D.; Zhang, C.; Hsu, J.W.P.; Wallace, R.M.; Cho, K. Intrinsic Air Stability Mechanisms of Two-Dimensional Transition Metal Dichalcogenide Surfaces: Basal versus Edge Oxidation. *2D Mater.* **2017**, *4*, 025050. [[CrossRef](#)]
51. Pető, J.; Ollár, T.; Vancsó, P.; Popov, Z.I.; Magda, G.Z.; Dobrik, G.; Hwang, C.; Sorokin, P.B.; Tapasztó, L. Spontaneous Doping of the Basal Plane of MoS₂ Single Layers through Oxygen Substitution under Ambient Conditions. *Nat. Chem.* **2018**, *10*, 1246–1251. [[CrossRef](#)]
52. Lu, H.; Kummel, A.; Robertson, J. Passivating the Sulfur Vacancy in Monolayer MoS₂. *APL Mater.* **2018**, *6*, 066104. [[CrossRef](#)]
53. Passler, N.C.; Paarmann, A. Generalized 4 × 4 Matrix Formalism for Light Propagation in Anisotropic Stratified Media: Study of Surface Phonon Polaritons in Polar Dielectric Heterostructures. *J. Opt. Soc. Am. B* **2017**, *34*, 2128. [[CrossRef](#)]
54. Kretschmann, E.; Raether, H. Notizen: Radiative Decay of Non Radiative Surface Plasmons Excited by Light. *Z. Nat. A* **1968**, *23*, 2135–2136. [[CrossRef](#)]
55. Stebunov, Y.V.; Arsenin, A.V.; Volkov, V.S. Chapter 12. Chemically Derived Graphene for Surface Plasmon Resonance Biosensing. In *Chemically Derived Graphene: Functionalization, Properties and Applications*; Nanoscience & Nanotechnology Series; Zhang, J., Ed.; Royal Society of Chemistry: London, UK, 2018; Volume 46, pp. 328–353. ISBN 9781788010801.
56. Stebunov, Y.V.; Aftenieva, O.A.; Arsenin, A.V.; Volkov, V.S. Highly Sensitive and Selective Sensor Chips with Graphene-Oxide Linking Layer. *ACS Appl. Mater. Interfaces* **2015**, *7*, 21727–21734. [[CrossRef](#)] [[PubMed](#)]